RSC Advances

PAPER

View Article Online
View Journal | View Issue

Cite this: *RSC Adv.*, 2019, **9**, 13372

Aza-BODIPY probe for selective visualization of cyclooxygenase-2 in cancer cells†

Thitima Pewklang,‡[a] Kantapat Chansaenpak,‡[b] Rung-Yi Lai,[a] Parinya Noisa[c] and Anyanee Kamkaew*[a]

Received 14th March 2019
Accepted 26th April 2019

DOI: 10.1039/c9ra01948k

rsc.li/rsc-advances

AZB-IMC$_2$ was developed as a COX-2 specific probe that exhibited a brighter fluorescence signal in cancer cells that overexpress COX-2 compared to normal cells. Oxidative stress agent-treated inflamed cell lines inducing high COX-2 levels revealed an enhanced fluorescence signal. Inhibitory studies showed a markedly reduced fluorescence intensity in cancer cells. The results suggested that **AZB-IMC$_2$** could be developed as a promising molecular tool for imaging guiding during surgery.

Introduction

Cyclooxygenase (COX), a prostaglandin-endoperoxide synthase, is a family of the two isoenzymes, COX-1 and COX-2, and plays an essential role in the formation of prostanoids.[1] Among the isoenzymes, clinical data revealed that COX-2 is overexpressed in all stages of cancer, from the earliest premalignant phase to metastasis[2] and high levels of COX-2 were found to be upregulated in various types of cancers, such as pancreatic, colon, gastric, stomach, breast, head/neck carcinoma, or inflammatory lesions.[3–11] Therefore, COX-2 has been considered as a promising target for tumor-specific target-based therapeutics.[6,12–18] In the past decades, some fluorescence-based COX-2-targeting probes have been developed,[19–25] however, COX-2-specific cancer biomarker development is still needed for clinical use.

Indomethacin (IMC), a commercially available nonsteroid anti-inflammatory drug (NSAID), exerts tumor-selective diagnosis and therapeutic potency by targeting COX-derived prostaglandin (PG) biosynthesis.[26,27] Although IMC is a non-selective COX isoforms inhibitor (COX-1 and COX-2), it becomes more selective after conjugation with fluorescent dyes.[6,24,28–31] For example, indomethacin (IMC) was linked to Nile Blue dye using a hexanediamine linker as a NIR fluorescent imaging probe.[30] The probe showed Golgi localization in cancer cells that overexpressed COX-2. Moreover, this NIR probe preferentially labeled the tumors *in vivo*, suggesting potential tool for imaging guided surgery. Another study employed a quinolinium-based moiety conjugated to IMC using click chemistry and the conjugate showed remarkable targeted ability towards cancer cells over normal cells regarding the COX-2 levels.[29]

In general, dyes that absorb and emit light in NIR region are ideal to minimize interference from cells autofluorescence, which is a major background noise in cell imaging. However, most currently used NIR-emitting dyes in bioimaging, particularly cyanine-based fluorophores, suffer from inherently low chemical and photostability.[32–34] These phenomena significantly limit the use of these dyes in long-term optical imaging that requires duration of light exposure in cellular environment. Borondipyrromethenes (BODIPYs) and their derivatives, in comparison, contain boron bridge that introduces rigidity to the system leading to prevention of *trans–cis* isomerization and twisting, enhancing fluorescent quantum yield and photostability of the dyes.[35–38]

According to the bivalent ligand approach, it was found that duplication pharmacophores leads to an increase in potency of binding recognition compared to the corresponding monovalent ligand.[39–44] Therefore, in this study, we reported bivalent conjugation of indomethacin to an aza-borondipyrromethene (aza-BODIPY) dye, a class of BODIPYs with NIR emission,[45] to enhance COX-2 selectivity (**AZB-IMC$_2$**).

Aza-BODIPY dye was linked to two molecules of indomethacin using azidotriethyleneglycol linker (Scheme 1). **AZB-IMC$_2$** has advantages of optical properties with NIR absorption ($\lambda_{max} \sim 700$ nm) and emission ($\lambda_{max} \sim 730$ nm) which can detect cancer cells by fluorescence imaging. NIR fluorescent COX-2 inhibitors are attractive candidates as deep-seated tissue targeted imaging agents. Such compounds are nonradioactive and stable, thus, they can be developed conveniently for clinical imaging agents.

Results and discussion

Synthesis of AZB-IMC$_2$

AZB-IMC$_2$ was synthesized according to Scheme 1. Compound **2** was obtained from the reaction of sodium azide with 2-(2-(2-

[a]*School of Chemistry, Institute of Science, Suranaree University of Technology, Nakhon Ratchasima, Thailand 30000. E-mail: anyanee@sut.ac.th*

[b]*National Nanotechnology Center, National Science and Technology Development Agency, Thailand Science Park, Pathum Thani, Thailand 12120*

[c]*Laboratory of Cell-Based Assays and Innovations, School of Biotechnology, Institute of Agricultural Technology, Suranaree University of Technology, Nakhon Ratchasima, Thailand 30000*

† Electronic supplementary information (ESI) available: Detailed synthesis and characterizations of **AZB-IMC$_2$**. See DOI: 10.1039/c9ra01948k

‡ These authors contributed equally to this article.

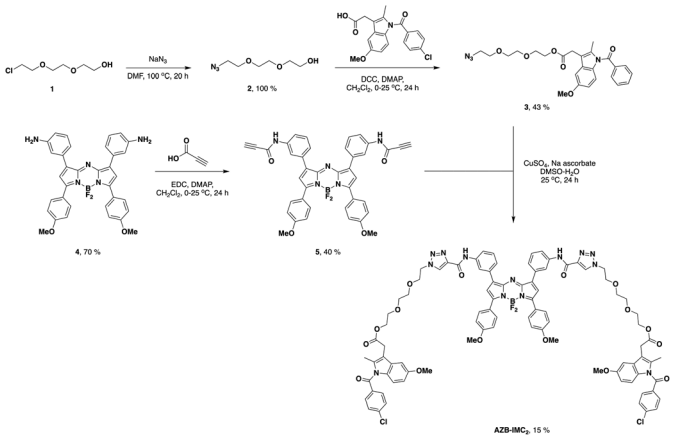

Scheme 1 Synthesis of AZB-IMC$_2$.

chloroethoxy)ethoxy)ethanol that give quantitative yield.[46] After that, **2** was undergone esterification with indomethacin to give compound **3**. In another part, amino aza-BODIPY **4** [47] was amide coupled with propiolic acid to obtain alkyne substituted aza-BODIPY **5**. Finally, the azide–alkyne Huisgen cycloaddition between the azide **3** and the alkyne **5** was performed to give **AZB-IMC$_2$** which was used as a COX-2 specific probe for cancer cells imaging.

Optical properties

AZB-IMC$_2$ showed strong UV-vis-NIR absorption peaking at 704 nm and emitted bright fluorescence peaking at 734 nm in DMSO (Fig. 1). The optical properties were determined under various conditions (DMSO, $CHCl_3$, H_2O + 3% Tween-80 and 0.01 M PBS pH 7.4 + 3% Tween-80) however, the absorption and emission maxima did not shift significantly. In water and PBS media, Tween-80, the biocompatible surfactant, was added to increase solubility of the dye (see ESI†). **AZB-IMC$_2$** exhibited high quantum yield in organic solvents, whereas low quantum yield was observed in aqueous media (Table 1). This might be the results from hydrophobic nature of the targeting probe leading to aggregation in aqueous medium. As **AZB-IMC$_2$** could absorb and emit lights in NIR region, this could be beneficial for deep tissue imaging.

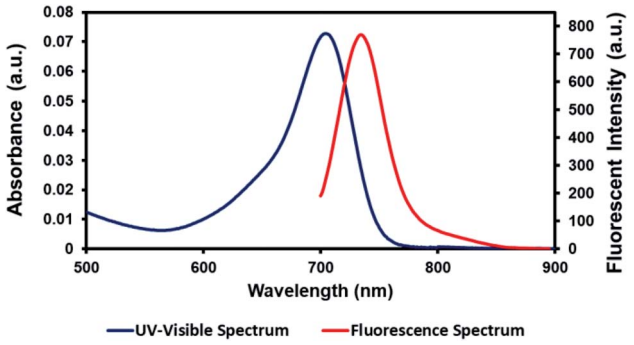

Fig. 1 UV-vis-NIR absorption and fluorescent spectra of AZB-IMC$_2$ (2.9 μM) excited at 670 nm in DMSO.

Table 1 Photophysical properties of AZB-IMC$_2$

Solvent	λ_{max} (nm)	ε (M^{-1} cm^{-1})	λ_{emiss} [a] (nm)	$\Delta\lambda$ (nm)	Φ_f [b]
DMSO	704	2.5×10^{-4}	734	30	0.47
$CHCl_3$	694	2.5×10^{-4}	722	28	0.80
H_2O [c]	710	1.7×10^{-4}	725	15	0.01
PBS [c] pH 7.4	710	1.5×10^{-4}	725	15	0.05

[a] Samples were excited at 670 nm. [b] Relative to Zn-phthalocyanine in pyridine ($\Phi_f = 0.30$). [c] With 3% Tween-80.

Cell viability

Next, cell viability of **AZB-IMC$_2$** were tested in different cell lines including cancer (HeLa, HepG2 and MCF-7) and normal (Hek293, RAW 264.7 and HFF) cells. The cells were treated with various concentrations of **AZB-IMC$_2$** ranging from 0–50 μM for 24 h before quantifying cell viability. Fig. 2 showed all the cells remained more than 80% viability at the concentration up to 20 μM while at higher concentration (50 μM) the cell viability reduced to only 50%. This phenomenon might be due to the aggregation of the probe at high concentration. However, the highest concentration we used in the following experiments was 5 μM which all the cells maintained full viability.

Confocal imaging

COX-2-targeting ability of **AZB-IMC$_2$** was then investigated in living cells. We selected 6 different cell lines, cancer cells (HeLa, HepG2 and MCF-7) known to overexpress COX-2 and normal cells with lower expression of COX-2 (HEK293, HFF and RAW 264.7).[19,24,25,30,48] After all the cells exposed to **AZB-IMC$_2$**, increased fluorescent signals were observed when the time increased. Moreover, the brighter fluorescence was detected in cancer cells compared to normal cells and the differences were obviously observed after 6 h incubation (Fig. 3).

In addition, in cancer cells, the fluorescence was found to be in dose-dependent manner (Fig. 4). We also noticed that 5 μM of **AZB-IMC$_2$** was enough for cell internalization and could be used as an indicator to distinguish cancer from normal cell lines.

Fluorescence images of lipopolysaccharide-induced inflammatory cell lines

To expand an application of **AZB-IMC$_2$** to detect intracellular COX-2 inflamed cells, HEK-293, RAW 264.7 and fibroblast (HFF)

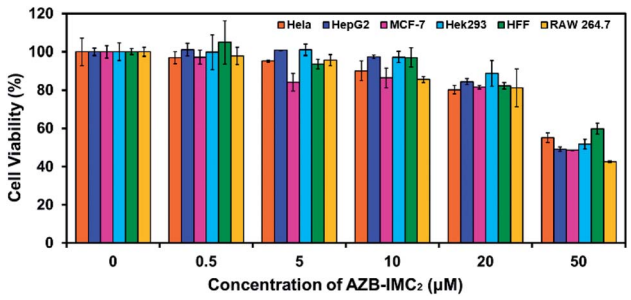

Fig. 2 Effect of AZB-IMC$_2$ on cell viability in different cell lines. All cells were treated with AZB-IMC$_2$ at different concentrations for 24 h.

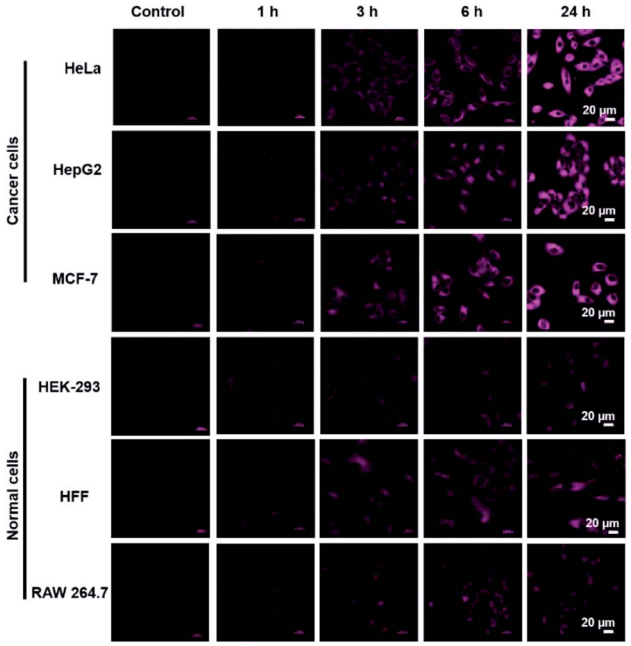

Fig. 3 Confocal and fluorescence microscopy images of AZB-IMC$_2$ (5 μM) depend on incubation time (1, 3, 6, and 24 h).

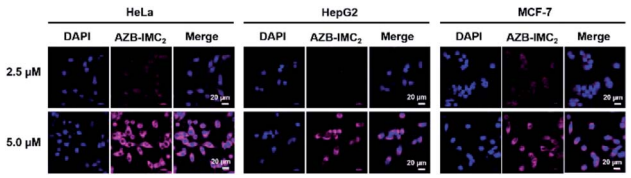

Fig. 4 Confocal images of dose-dependent effect of AZB-IMC$_2$ (2.5 and 5.0 μM) in HeLa, HepG2, and MCF-7 cells, which were incubated for 3 h.

cell lines were first induced with LPS (lipopolysaccharides) to upregulate COX-2 levels. After incubation with LPS for 12 h, followed by treatment with **AZB-IMC$_2$** for 2 h, an enhanced fluorescence was observed in all cell lines (Fig. 5), indicating that **AZB-IMC$_2$** could be used to monitor the oxidative stress in the living system.

COX-2 inhibition experiment

Moreover, to evaluate the selectivity towards cancer cells over normal cells *via* COX-2 mediated endocytosis upon binding to

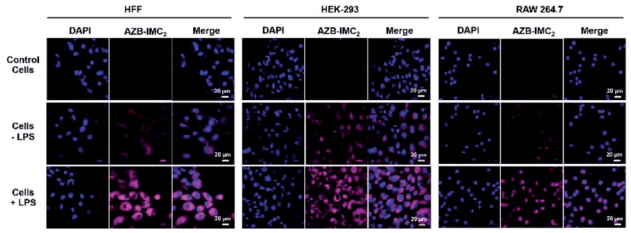

Fig. 5 Confocal images of LPS-induced inflammation cell lines. HFF, HEK-293 and RAW 264.7 were incubated with LPS (1 μg mL^{-1}) for 12 h before exposing to AZB-IMC$_2$ (5 μM) for 2 h. The fluorescent signals enhanced in the LPS-induced oxidative stress cells.

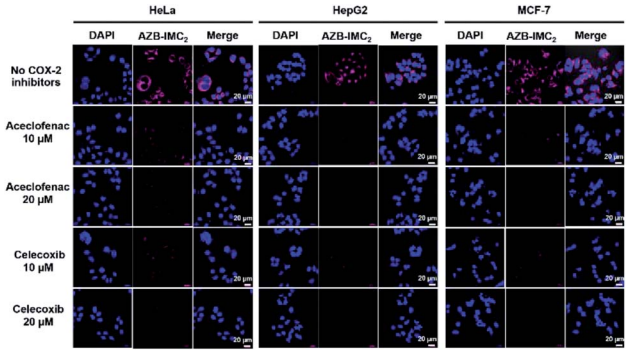

Fig. 6 Confocal images of COX-2 inhibitory effect. Cancer cells were incubated with COX-2 specific inhibitors (aceclofenac and celecoxib, 10 μM and 20 μM) for 3 h, then incubated with AZB-IMC$_2$ (5 μM) for another 3 h.

indomethacin units, the COX-2 blocking experiments were performed. Cancer cells were incubated with 10 μM and 20 μM of potent COX-2 specific inhibitors (aceclofenac and celecoxib)[49,50] for 3 h to down-regulate COX-2 levels before adding **AZB-IMC$_2$**. Fig. 6 shows that all cancer cells (HeLa, HepG2 and MCF-7) incubated with **AZB-IMC$_2$** in the absence of COX-2 inhibitors exhibited bright fluorescence, whereas, a significant reduction in the fluorescent intensity was observed when the cells exposed to COX-2 inhibitors prior to **AZB-IMC$_2$** treatment. Moreover, the fluorescence intensity decreased with increasing amount of celecoxib and aceclofenac, implying that celecoxib and aceclofenac prevented the labeling of cancer cells by **AZB-IMC$_2$**. Therefore, the indomethacin-conjugated probe **AZB-IMC$_2$** displayed a clear relationship with COX-2 expression levels.

Conclusions

In summary, we successfully developed the COX-2 specific probe (**AZB-IMC$_2$**) for NIR cancer imaging. **AZB-IMC$_2$** contained two moieties of indomethacin showing strong absorption and fluorescence in the NIR region (above 700 nm). **AZB-IMC$_2$** was not harmful to both cancer (HeLa, HepG2 and MCF-7) and normal (Hek293, RAW 264.7 and HFF) cells at the concentration up to 20 μM. Moreover, as shown in confocal images, **AZB-IMC$_2$** exhibited high selectivity towards cancer cells where COX-2 is overexpressed after at least 3 h incubation. In addition, LPS-treated inflamed cell lines (Hek293, RAW 264.7 and HFF) showed enhanced fluorescence as COX-2 level was upregulated. On the other hand, inhibition of COX-2 levels in cancer cells caused significant decreasing of fluorescent signals. These results confirmed that **AZB-IMC$_2$** responded to COX-2 expression level of the cells, which can be useful in development of a COX-2-specific cancer biomarker for clinical applications.

Experimental

Materials and instruments

All glassware was oven-dried prior to use. All the reagents have been purchased from the commercially sources (Sigma Aldrich, TCI, Carlo Erba, Acros, Merck) and used without further

purification. Column chromatography purifications were performed using silica gel for chromatography (Carlo Erba) as a stationary phase. Analytical thin layer chromatography (TLC) was performed on TLC Silica gel 60 F254 (Merck) and visualized with UV cabinet. ^{1}H NMR and ^{13}C NMR spectra were recorded on Bruker-500 MHz spectrometer at room temperature. Chemical shifts of ^{1}H NMR spectra were recorded and reported in ppm from the solvent resonance ($CDCl_3$ at 7.24 ppm). Data are reported as follows: chemical shift, multiplicity (s = singlet, d = doublet, t = triplet, m = multiplet), coupling constants, and number of protons. ^{13}C NMR spectra were also recorded in ppm from the solvent resonance ($CDCl_3$ at 77.23 ppm). MS were measured under ESI and MALDI conditions.

Synthetic procedures

Synthesis of 2-(2-(2-azidoethoxy)ethoxy)ethyl-2-(1-benzoyl-5-methoxy-2-methyl-1*H*-indol-3-yl)acetate (3). To solution of **2** (0.2498 g, 1.474 mmol) in dry dichloromethane (DCM, 5 mL) was added indomethacin (0.4904 g, 1.371 mmol). The reaction mixture was cooled to 0 °C. Then, *N*,*N*′-dicyclohexylcarbodiimide (DCC, 0.4400 g, 2.132 mmol) and 4-dimethylaminopyridine (DMAP, 48.2 mg, 0.394 mmol) were added into the mixture at 0 °C. The reaction mixture was allowed to warm to room temperature and stirred for 24 h. After that, the reaction was filtered through Celite® with DCM as eluent. The organic layer was washed with DI water (3 × 20 mL) and brine (20 mL), and dried over anhydrous Na_2SO_4. The solvent was then removed under reduced pressure. The obtained residue was purified by silica chromatography eluting with DCM : MeOH (100 : 0 to 90 : 10) to yield 0.3062 g (43%) of **3** as a yellow sticky oil. ^{1}H NMR (500 MHz, $CDCl_3$): δ = 7.62 (d, J = 8.5 Hz, 2H), 7.43 (d, J = 8.4 Hz, 2H), 6.94 (d, J = 2.4 Hz, 1H), 6.85 (d, J = 9.0 Hz, 1H), 6.64–6.62 (m, 1H), 4.24 (t, J = 9.5 Hz, 2H), 3.80 (s, 3H), 3.66 (s, 2H), 3.60 (t, J = 10.1 Hz, 2H), 3.56 (s, 4H), 3.32 (t, J = 10.0 Hz, 2H), 2.34 (s, 3H), 2.19 (s, 2H). ^{13}C NMR (500 MHz, $CDCl_3$): δ = 170.9, 168.3, 156.1, 139.3, 136.1, 134.0, 131.2, 131.2, 129.2, 115.0, 112.6, 111.7, 101.5, 70.7, 70.6, 70.1, 69.2, 64.2, 55.8, 50.7, 30.3, 13.5 ppm. MS (ESI+) *m*/*z*: the calculated value (calcd) for ($[M + Na]^+$): 537.15, found 537.15.

Synthesis of *N*,*N*′-((5,5-difluoro-3,7-bis(4-methoxyphenyl)-5*H*-4l4,5l4-dipyrrolo[1,2-*c*:2′,1′-*f*][1,3,5,2]triazaborinine-1,9-diyl)bis(3,1-phenylene))dipropiolamide (5). To solution of **4** (145 mg, 0.247 mmol) in dry dichloromethane (DCM, 5 mL) was added propiolic acid (0.06 mL, 1 mmol, 8.6 eq.). The reaction mixture was then cooled to 0 °C. 1-Ethyl-3-(3-dimethylaminopropyl) carbodiimide (EDC, 200 mg, 1.04 mmol) and 4-dimethylaminopyridine (DMAP, 30 mg, 0.24 mmol) were added into the mixture at 0 °C. The reaction mixture was allowed to warm to room temperature and stirred for 24 h. After that, the reaction was filtered through Celite® with DCM as eluent. The organic layer was washed with HCl (0.2 N, 1 × 20 mL), NaOH (0.2 N, 2 × 20 mL) and brine (20 mL), respectively. The organic layer was then dried over anhydrous Na_2SO_4 and the solvent was removed under reduced pressure. The obtained residue was purified by silica chromatography eluting with hexane : EtOAc (1 : 1 to 1 : 3) to yield 69 mg (40%) of **5** as a dark green solid. ^{1}H NMR (500 MHz, $CDCl_3$): δ = 8.50 (s, 1H), 8.03–8.01 (m, 2H), 7.90 (d J = 8.7 Hz, 1H), 7.74–7.68 (m, 1H), 7.50 (s, 1H), 7.39–7.37 (m, 1H), 6.96 (d, J = 8.7 Hz, 2H), 6.64 (s, 1H), 3.86 (s, 3H), 2.97 (s, 1H). ^{13}C NMR (500 MHz, $CDCl_3$): δ = 162.3, 161.2, 150.0, 145.4, 142.2, 137.6, 133.5, 132.0, 131.4, 129.5, 126.1, 121.2, 119.4, 114.5, 114.1, 75.4, 74.8, 55.7 ppm. MS (MALDI-TOF) *m*/*z*: the calculated value (calcd) for $C_{40}H_{28}BF_2N_5NaO_4$ ($[M + Na]^+$): 714.21, $C_{40}H_{28}BF_2KN_5O_4$ ($[M + K]^+$): 730.18, found 714.27, 730.23.

Synthesis of (((((((((5,5-difluoro-3,7-bis(4-methoxyphenyl)-5*H*-4l4,5l4-dipyrrolo[1,2-*c*:2′,1′-*f*][1,3,5,2]triazaborinine-1,9-diyl)bis(3,1-phenylene))bis(azanediyl))bis(carbonyl))bis(1*H*-1,2,3-triazole-4,1-diyl))bis(ethane-2,1-diyl))bis(oxy))bis(ethane-2,1-diyl))bis(oxy))bis(-ethane-2,1-diyl)-bis(2-(1-(4-chlorobenzoyl)-5-methoxy-2-methyl-1*H*-indol-3-yl)acetate) (AZB-IMC$_2$). **5** (54 mg, 0.078 mmol) and **3** (0.1178 g, 0.2287 mmol, 3 eq.) were dissolved in dimethyl sulfoxide (DMSO, 5 mL). To the reaction mixture was added sodium ascorbate (0.2 mmol, 400 μL of freshly prepared 0.5 M solution in DI water) and copper(II) sulfate pentahydrate (0.12 mmol, 240 μL of freshly prepared 0.5 M solution in DI water), respectively. The resulting mixture was stirred vigorously at room temperature for 24 h. After that, DCM (20 mL) was added to the mixture and the organic layer was washed with DI water (3 × 20 mL). The DCM layer was then dried over anhydrous Na_2SO_4 and the solvent was removed under reduced pressure. The obtained residue was purified by silica chromatography eluting with hexane : EtOAc (1 : 1 to 1 : 3), followed by DCM : MeOH (95 : 5) to yield 20 mg (15%) of **AZB-IMC$_2$** as a dark green solid. ^{1}H NMR (500 MHz, $CDCl_3$): δ = 8.97 (s, 1H), 8.35 (s, 1H), 8.29 (s, 1H), 8.08 (d, J = 8.8 Hz, 2H), 7.84 (d, J = 7.8 Hz, 1H), 7.68 (d, J = 7.9 Hz, 2H), 7.59 (s, 1H), 7.57 (s, 1H), 7.45–7.40 (m, 1H), 7.07 (s, 1H), 6.98 (d, J = 8.8 Hz, 2H), 6.92 (s, 1H), 6.81 (d, J = 9.0 Hz, 2H), 6.60 (d, J = 8.9 Hz, 1H), 4.58 (s, 2H), 4.26 (t, J = 4.6 Hz, 2H), 4.05–4.04 (m, 2H), 3.87 (s, 3H), 3.81 (m, 2H), 3.76 (s, 3H), 3.66–3.63 (m, 2H), 3.54–3.52 (m, 2H), 3.45 (t, J = 3.7 Hz, 2H), 2.31 (s, 3H). ^{13}C NMR (500 MHz, $CDCl_3$): δ = 171.2, 168.6, 162.3, 158.5, 158.4, 157.1, 156.3, 143.6, 139.6, 138.2, 136.4, 134.2, 133.6, 132.1, 131.5, 131.0, 129.6, 129.4, 127.4, 125.8, 124.5, 121.1, 120.7, 119.4, 115.2, 114.6, 112.8, 112.0, 111.8, 101.9, 70.9, 70.8, 69.5, 64.4, 56.0, 34.3, 34.3, 30.5, 30.0, 13.7 ppm. MS (MALDI-TOF) *m*/*z*: the calculated value (calcd) for $C_{90}H_{83}BCl_2FN_{13}NaO_{16}$ ($[M - F + H]^+$): 1701.55, $C_{90}H_{82}BCl_2F_2N_{13}NaO_{16}$ ($[M + Na]^+$): 1742.53, $C_{90}H_{82}BCl_2F_2KN_{13}O_{16}$ ($[M + K]^+$): 1758.51, found 1701.83, 1742.87, 1758.84.

UV/vis and fluorescence spectroscopic methods

All the UV/vis absorption spectra and fluorescence were recorded on UV-vis Spectrophotometer (Agilent Technologies Cary 300) and Spectrofluorometer (PerkinElmer LS55), respectively. In both experiments, stock solutions (350 μM) of **AZB-IMC$_2$** probe was prepared in DMSO. 10 μM solutions of probes in chloroform, DMSO, DI water, and 0.01 M PBS buffer (pH 7.4) with 3% DMSO were prepared as working solutions. For fluorescence experiments, the emission spectra were recorded at excitation wavelength of 670 nm.

Cell culture

Human cervical cancer (HeLa), human hepatoma cell cancer (HepG2), Michigan Cancer Foundation-7 (MCF-7), human

embryonic kidney 293 (HEK-293), Human Foreskin Fibroblast (HFF), and RAW264.7 cell lines were cultured on 75 cm^3 culture flasks in Dulbecco's Modified Eagle's Media (Hyclone) supplemented with 10% fetal bovine serum (Gibco) and 1% penicillin–streptomycin (Corning). All the cells were cultured at 37 °C in a humidified 95% air, 5% CO_2 atmosphere.

Cell viability assay

The cells were seeded on 96-well plate approximately 7×10^3 cells per well and incubated in completed media for 24 h. Thereafter, the cells were treated with 0, 0.5, 5, 10, 20, 50 μM of **AZB-IMC$_2$** and continued culturing for 24 h. After incubation, the cells were washed with 0.01 M PBS (3 times) and treated with 20 μL of methylthiazolyldiphenyl-tetrazolium bromide (MTT reagent, 0.5 mg mL^{-1}, Sigma-Aldrich) for 2 h. After media removal, DMSO was added to dissolve formazan product. The cell's viabilities were detected through UV-vis absorption of formazan at wavelength 560 nm.

Time dependent internalization

HeLa, HepG2, MCF-7, HEK-293, HFF and RAW 294.7 cells, approximately 1×10^4 cells, were seeded on 8-well chambered coverglass (LabTek, Nunc) and incubated in completed media for 24 h. After that, the cells were treated with 5 μM of **AZB-IMC$_2$** for 0, 1, 3, 6, 24 h. After incubation, the cells were washed with 0.01 M PBS (3 times) and treated with 0.5 μg mL^{-1} of Hoechst 33342 containing media. The cells were imaged by Laser Scanning Confocal Microscope (Nikon A1Rsi).

Dose dependent internalization

HeLa, HepG2, MCF-7 cells, approximately 1×10^4 cells, were seeded on 8-well chambered coverglass and incubated in completed media for 24 h. After that, the cells were treated with 2.5 and 5.0 μM of **AZB-IMC$_2$** probe for 3 h. After incubation, the cells were washed with 0.01 M PBS (3 times) and treated with 0.5 μg mL^{-1} of Hoechst 33342 containing media. The cells were visualized by Laser Scanning Confocal Microscope (Nikon A1Rsi).

LPS-induced inflammation experiment

To study inflammation effects, HEK-293, HFF and RAW 294.7 were seeded on 8-well chambered coverglass and incubated for 24 h. After that, the cells were treated with 1 μg mL^{-1} lipopolysaccharides (LPS, O111:B4, Sigma) in DMEM for 12 h. After incubation in LPS containing media, the cells were washed three times with 0.01 M PBS and treated with 5 μM of **AZB-IMC$_2$** for 2 h. Before imaging, the cells were washed three times with 0.01 M PBS and treated with 0.5 μg mL^{-1} of Hoechst 33342 containing media.

COX-2 blocking experiment

To study inhibition effect of COX-2 with blocking, HeLa, HepG2, and MCF-7 cells were incubated with 10 μM and 20 μM of aceclofenac and celecoxib (Tokyo Company Industry) for 3 h before being treated with 5 μM of **AZB-IMC$_2$** and incubated for another 3 h. Thereafter, the cells were washed with 0.01 M PBS three times and treated with 0.5 μg mL^{-1} of Hoechst 33342 containing media before visualization by Laser Scanning Confocal Microscope (Nikon A1Rsi).

Conflicts of interest

There are no conflicts to declare.

Acknowledgements

This research was supported by SUT Research and Development Fund.

Notes and references

1 F. A. Fitzpatrick, *Curr. Pharm. Des.*, 2004, **10**, 577–588.
2 K. Subbaramaiah and A. J. Dannenberg, *Trends Pharmacol. Sci.*, 2003, **24**, 96–102.
3 M. Breinig, P. Schirmacher and M. A. Kern, *Curr. Pharm. Des.*, 2007, **13**, 3305–3315.
4 K. Echizen, O. Hirose, Y. Maeda and M. Oshima, *Cancer Sci.*, 2016, **107**, 391–397.
5 M. J. Edelman, L. Hodgson, X. Wang, R. A. Kratzke and E. E. Vokes, *J. Clin. Oncol.*, 2012, **30**, 2019–2020.
6 H. S. Kim, A. Sharma, W. X. Ren, J. Han and J. S. Kim, *Biomaterials*, 2018, **185**, 63–72.
7 M. L. Nasi and M. Castiglione, *Ann. Oncol.*, 2002, **13**, 1169–1171.
8 S. Nath, L. D. Roy, P. Grover, S. Rao and P. Mukherjee, *Pancreas*, 2015, **44**, 909–917.
9 A. Thiel, J. Mrena and A. Ristimaki, *Cancer Metastasis Rev.*, 2011, **30**, 387–395.
10 D. Wang and R. N. Dubois, *Oncogene*, 2010, **29**, 781–788.
11 Z. Khan, N. Khan, R. P. Tiwari, N. K. Sah, G. Prasad and P. S. Bisen, *Curr. Drug Targets*, 2011, **12**, 1082–1093.
12 R. de Souza Pereira, *Recent Pat. Anticancer Drug Discov.*, 2009, **4**, 157–163.
13 E. F. de Vries, *Curr. Pharm. Des.*, 2006, **12**, 3847–3856.
14 J. F. Evans and S. L. Kargman, *Curr. Pharm. Des.*, 2004, **10**, 627–634.
15 H. R. Herschman, J. J. Talley and R. DuBois, *Mol. Imaging Biol.*, 2003, **5**, 286–303.
16 L. Milas, *Am. J. Clin. Oncol.*, 2003, **26**, S66–S69.
17 K. Chansaenpak, M. Wang, S. Liu, Z. Wu, H. Yuan, P. S. Conti, Z. Li and F. P. Gabbaï, *RSC Adv.*, 2016, **6**, 23126–23133.
18 K. Chansaenpak, B. Vabre and F. P. Gabbaï, *Chem. Soc. Rev.*, 2016, **45**, 954–971.
19 A. Bhardwaj, J. Kaur, F. Wuest and E. E. Knaus, *ChemMedChem*, 2014, **9**, 109–116.
20 Y. Ti, L. Yu, Y. Tang, T. Jin, M. Yang, R. Wang, Y. Xu and W. Zhu, *Sens. Actuators, B*, 2018, **265**, 582–590.
21 M. J. Uddin, B. C. Crews, A. L. Blobaum, P. J. Kingsley, D. L. Gorden, J. O. McIntyre, L. M. Matrisian, K. Subbaramaiah, A. J. Dannenberg, D. W. Piston and L. J. Marnett, *Cancer Res.*, 2010, **70**, 3618–3627.

22 M. J. Uddin, B. C. Crews, K. Ghebreselasie and L. J. Marnett, *Bioconjugate Chem.*, 2013, **24**, 712–723.
23 H. Zhang, J. Fan, J. Wang, B. Dou, F. Zhou, J. Cao, J. Qu, Z. Cao, W. Zhao and X. Peng, *J. Am. Chem. Soc.*, 2013, **135**, 17469–17475.
24 H. Zhang, J. Fan, J. Wang, S. Zhang, B. Dou and X. Peng, *J. Am. Chem. Soc.*, 2013, **135**, 11663–11669.
25 Q. Zhang, Z. Han, J. Tao, W. Zhang, P. Li, L. Tang and Y. Gu, *J. Biophotonics*, 2018, **11**, e201700339.
26 R. J. Flower, *Nat. Rev. Drug Discovery*, 2003, **2**, 179–191.
27 M. G. Papich, in *Saunders Handbook of Veterinary Drugs*, ed. M. G. Papich and W. B. Saunders, St. Louis, 2016, pp. 396–397, DOI: 10.1016/b978-0-323-24485-5.00307-7.
28 J. H. Jang, H. Lee, A. Sharma, S. M. Lee, T. H. Lee, C. Kang and J. S. Kim, *Chem. Commun.*, 2016, **52**, 9965–9968.
29 H. S. Kim, T. Park, W. X. Ren, J. Y. Lim, M. Won, J. S. Heo, S. G. Lee and J. S. Kim, *Dyes Pigm.*, 2018, **150**, 261–266.
30 B. Wang, J. Fan, X. Wang, H. Zhu, J. Wang, H. Mu and X. Peng, *Chem. Commun.*, 2015, **51**, 792–795.
31 H. Zhang, J. Fan, K. Wang, J. Li, C. Wang, Y. Nie, T. Jiang, H. Mu, X. Peng and K. Jiang, *Anal. Chem.*, 2014, **86**, 9131–9138.
32 C. Shi, J. B. Wu and D. Pan, *Review on near-infrared heptamethine cyanine dyes as theranostic agents for tumor imaging, targeting, and photodynamic therapy*, SPIE, 2016.
33 S. Luo, E. Zhang, Y. Su, T. Cheng and C. Shi, *Biomaterials*, 2011, **32**, 7127–7138.
34 S. A. Soper and Q. L. Mattingly, *J. Am. Chem. Soc.*, 1994, **116**, 3744–3752.
35 A. Kamkaew, S. H. Lim, H. B. Lee, L. V. Kiew, L. Y. Chung and K. Burgess, *Chem. Soc. Rev.*, 2013, **42**, 77–88.
36 A. Loudet and K. Burgess, *Chem. Rev.*, 2007, **107**, 4891–4932.
37 N. Boens, V. Leen and W. Dehaen, *Chem. Soc. Rev.*, 2012, **41**, 1130–1172.
38 R. Ziessel, G. Ulrich and A. Harriman, *New J. Chem.*, 2007, **31**, 496–501.
39 A. P. Tamiz, J. Zhang, M. Zhang, C. Z. Wang, K. M. Johnson and A. P. Kozikowski, *J. Am. Chem. Soc.*, 2000, **122**, 5393–5394.
40 M. Rosini, E. Simoni, M. Bartolini, E. Soriano, J. Marco-Contelles, V. Andrisano, B. Monti, M. Windisch, B. Hutter-Paier, D. W. McClymont, I. R. Mellor and M. L. Bolognesi, *ChemMedChem*, 2013, **8**, 1276–1281.
41 I. Raji, F. Yadudu, E. Janeira, S. Fathi, L. Szymczak, J. R. Kornacki, K. Komatsu, J. D. Li, M. Mrksich and A. K. Oyelere, *Bioorg. Med. Chem.*, 2017, **25**, 1202–1218.
42 P. S. Portoghese, *J. Med. Chem.*, 2001, **44**, 2259–2269.
43 S. Howorka, J. Nam, H. Bayley and D. Kahne, *Angew. Chem., Int. Ed. Engl.*, 2004, **43**, 842–846.
44 T. Birnkammer, A. Spickenreither, I. Brunskole, M. Lopuch, N. Kagermeier, G. Bernhardt, S. Dove, R. Seifert, S. Elz and A. Buschauer, *J. Med. Chem.*, 2012, **55**, 1147–1160.
45 Y. Ge and D. F. O'Shea, *Chem. Soc. Rev.*, 2016, **45**, 3846–3864.
46 Y. R. Baker, W. R. Galloway, J. T. Hodgkinson and D. R. Spring, *Molecules*, 2013, **18**, 11783–11796.
47 A. Kamkaew and K. Burgess, *Chem. Commun.*, 2015, **51**, 10664–10667.
48 G. Totzke, K. Schulze-Osthoff and R. U. Janicke, *Oncogene*, 2003, **22**, 8021–8030.
49 S. S. Solanki and R. Dahima, *J. Adv. Pharm. Technol. Res.*, 2011, **2**, 128–131.
50 J. L. Mateos, *Drugs Today*, 2010, **46**(suppl. A), 1–25.